

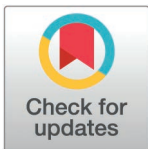
RESEARCH ARTICLE

Dynamics of X chromosome hyper-expression and inactivation in male tissues during stick insect development

Jelisaveta Djordjevic^{1*}, Patrick Tran Van^{1,2}, William Toubiana¹, Marjorie Labédan¹, Zoé Dumas¹, Jean-Marc Aury³, Corinne Cruaud⁴, Benjamin Istace³, Karine Labadie⁴, Benjamin Noel³, Darren J. Parker^{1,5}, Tanja Schwander^{1*}

1 Department of Ecology and Evolution, University of Lausanne, Lausanne, Switzerland, **2** Institut Curie, PSL Research University, INSERM, Paris, France, **3** Génomique Métabolique, Genoscope, Institut François Jacob, CEA, CNRS, Univ Evry, Université Paris-Saclay, Evry, France, **4** Genoscope, Institut François Jacob, CEA, Université Paris-Saclay, Evry, France, **5** School of Environmental and Natural Sciences, Bangor University, Bangor, United Kingdom

* jelisaveta.djordjevic@unil.ch (JD); tanja.schwander@unil.ch (TS)



OPEN ACCESS

Citation: Djordjevic J, Tran Van P, Toubiana W, Labédan M, Dumas Z, Aury J-M, et al. (2025) Dynamics of X chromosome hyper-expression and inactivation in male tissues during stick insect development. *PLoS Genet* 21(3): e1011615. <https://doi.org/10.1371/journal.pgen.1011615>

Editor: Colin Meiklejohn, University of Nebraska-Lincoln, UNITED STATES OF AMERICA

Received: July 16, 2024

Accepted: February 5, 2025

Published: March 10, 2025

Peer Review History: PLOS recognizes the benefits of transparency in the peer review process; therefore, we enable the publication of all of the content of peer review and author responses alongside final, published articles. The editorial history of this article is available here: <https://doi.org/10.1371/journal.pgen.1011615>

Copyright: © 2025 Djordjevic et al. This is an open access article distributed under the terms of the [Creative Commons Attribution License](https://creativecommons.org/licenses/by/4.0/), which permits unrestricted use, distribution, and reproduction in any medium, provided the original author and source are credited.

Abstract

Differentiated sex chromosomes are frequently associated with major transcriptional changes: the evolution of dosage compensation (DC) to equalize gene expression between the sexes and the establishment of meiotic sex chromosome inactivation (MSCI). Our study investigates the mechanisms and developmental dynamics of dosage compensation and meiotic sex chromosome inactivation in the stick insect species *T. poppense*. Stick insects are characterized by XX/X0 sex determination, with an X chromosome that likely evolved prior to the diversification of insects over 450 Mya. We generated a chromosome-level genome assembly and analyzed gene expression from various tissues (brain, gut, antennae, leg, and reproductive tract) across developmental stages in both sexes. Our results show that complete dosage compensation is maintained in male somatic tissues throughout development, mediated by upregulation of the single X chromosome. Contrarily, in male reproductive tissues, dosage compensation is present only in the early nymphal stages. As males reach the 4th nymphal stage and adulthood, X-linked gene expression diminishes, coinciding with the onset of meiosis and MSCI, which involves classical silencing histone modifications. These findings reveal the dynamic regulation of X-linked gene expression in *T. poppense*, and suggest that reduced X-expression in insect testes is generally driven by MSCI rather than an absence of dosage compensation mechanisms. Our work provides critical insights into sex chromosome evolution and the complex interplay of dosage compensation and MSCI across tissues and developmental stages.

Author summary

Males and females have often different numbers of sex chromosomes. For example, in humans, females have two X chromosomes, while males have one X and one Y. To avoid

Data availability statement: Genome assembly: PRJNA1126215; annotation and scripts to analyze data (https://github.com/JelisavetaDjordjevic/Dosage_compensation); raw sequence reads have been deposited in NCBI's sequence read archive under the following bioprojects: PRJEB76439 (reference genome), PRJNA1128554 (RNAseq reads), PRJNA1213497 (ChIP-seq), PRJNA1212995 (Hi-C). Data were processed to generate plots and statistics using R v3.4.4.

Funding: This study was funded by the European Research Council Consolidator Grant (ERC) (No Sex No Conflict to T.S.), the Swiss FNS grant 31003A_182495 (T.S.), Genoscope, the Commissariat à l'Énergie Atomique et aux Énergies Alternatives (CEA), France Génomique (ANR-10-INBS-09-08). The funders had no role in study design, data collection and analysis, decision to publish, or preparation of the manuscript.

Competing interests: The authors declare that they have no competing interests.

potential imbalances in gene expression from the sex chromosomes between males and females, many species have evolved dosage compensation mechanisms. However, little is known about how dosage compensation varies across tissues and during development. We investigated this variation in the stick insect *Timema poppense*, which has an XO system where males have one X chromosome and females have two (there is no Y chromosome). Our analysis of gene expression across tissues and developmental stages revealed consistent dosage compensation in somatic tissues but variation in testes. While dosage compensation is complete in early nymphal testes, it is replaced by X chromosome inactivation in later developmental stages and adulthood, resulting in imbalanced expression levels between sexes. These findings provide new insights into how sex chromosome regulation evolves across tissues and developmental stages.

Introduction

In species where sex is determined by differentiated sex chromosomes, sex chromosome copy number differs between males and females. For example, in XO and XY systems, males have only one copy of each gene located on the X chromosome, while females have two. Because gene copy number generally correlates with expression levels [1], the expression level of X-linked genes in males is expected to be half that of the same genes in females. However, selection can act on the regulation of expression in a sex-specific manner, and potentially restore similar expression levels in both sexes [2–4], a process known as dosage compensation [2,5,6]. The mechanisms underlying dosage compensation between the sexes vary with respect to whether sex chromosomes are downregulated in the homogametic sex, or upregulated in the heterogametic sex. Downregulation of X-linked expression in females underlies dosage compensation in eutherian mammals and the worm *Caenorhabditis elegans*: In eutherian mammals, females inactivate one of the X chromosomes in each cell [6,7], whereas in *C. elegans*, the expression of both X chromosome copies in hermaphrodites is reduced to achieve similar total expression levels as for the single X in males [8,9]. Upregulation of the single X in males appears to underlie dosage compensation in diverse insect species [10–13]. The ancestral sex determination system in insects was most likely XO/XX or XY/XX male heterogamety [14]. There is considerable conservation of X chromosome gene content in many insect orders, suggesting that there may be an ancient insect X chromosome which partially persisted for over 450 MYA [15]. However, X upregulation in males is documented for both, species with a conserved X chromosome content as well as species with novel X chromosomes [11,13,16–18], where it involves different molecular mechanisms for different species [19,20].

Interestingly, in all studied XO and XY species that feature dosage compensation via X upregulation in males, the single X in males is much less expressed in the testes than in the somatic tissues [11–13,21]. This is thought to be due to the presence of dosage compensation in somatic tissues and the absence of dosage compensation in the reproductive tissues, perhaps because the gene expression optima in male versus female gonads are so different that there is no or reduced selection for dosage compensation in this tissue [11]. Furthermore, transcriptional silencing of the X because of meiotic sex chromosome inactivation (MSCI) can specifically reduce the expression levels of X-linked genes in the testes of some species [22,23].

Beyond the specific case of testes in adult males, the extent of dosage compensation variation across tissues and development remains understudied [21,24]. Furthermore, the key mechanisms affecting X-linked expression in males (dosage compensation and meiotic sex chromosome inactivation) are only characterized for a few well-studied model organisms,

preventing inferences of conserved versus lineage-specific aspects of sex chromosome expression. Here we fill these knowledge gaps by exploring how the extent of dosage compensation varies over development in somatic and reproductive tissues as well as the potential impact of meiotic sex chromosome inactivation in the stick insect *Timema poppense*. These stick insects are characterized by XX:X0 sex determination [25] and an X chromosome content that is shared across many insect orders [15]. Previous work on *Timema* stick insects showed that in adults, there is dosage compensation in the head and legs, but not in the reproductive tract [13]. We generate a new chromosome-level genome assembly of *T. poppense* based on long-read sequencing and Hi-C scaffolding, and sequence RNA from brain, gut, antennae, leg and reproductive tract samples in males and females across development. We then assess the expression levels of genes located on the X chromosome(s) and autosomes in both sexes. Finally, we test for meiotic sex chromosome inactivation in the male germline via immunostaining and genome profiling for silencing histone marks, and discuss how MSCI globally affects X-linked gene expression patterns in male gonads.

Materials and methods

Sample collection and reference genome generation

We used wild-collected females of the species *T. poppense* (36°59'44.5"N 121°43'05.0"W) for generating the reference genome. We assembled contigs based on Nanopore and Illumina libraries (sequenced at 75x respectively 50x coverage) generated from a single female, and then scaffolded contigs using a Hi-C library (sequenced at 61x coverage) based on a different female. We annotated this assembly using transcriptome data from different tissues and development stages of male and female *T. poppense* as well as from a closely related species (*T. douglasi*; see Gene annotation section).

Sequencing libraries. To extract high molecular weight (HMW) DNA, we flash-froze a single female (without gut) in liquid nitrogen and ground it using a Cryomill (Retsch). We then extracted HMW DNA using a G/20 Genomic Tips kit (Qiagen) following the manufacturer's protocols. We checked DNA integrity on a pulse field agarose gel.

A total of four ONT libraries were prepared following Oxford Nanopore instructions. Four libraries were prepared using the SQK-LSK109 ligation sequencing kit and were loaded on four PromethION R9.4.1 Flow Cells. Flow Cell loading was performed according to the Oxford Nanopore protocol and resulted in 75X coverage.

A PCR free Illumina library (based on the same HMW extraction) was prepared using the Kapa Hyper Prep Kit (Roche, Basel, Switzerland), following manufacturer instructions. The library was quantified by qPCR using the KAPA Library Quantification Kit for Illumina Libraries (Roche), and the library profile was assessed using a High Sensitivity DNA kit on an Agilent Bioanalyzer (Agilent Technologies, Santa Clara, CA, USA). The library was then sequenced to approximately 50x coverage on an Illumina HiSeq 4000 instrument (Illumina, San Diego, CA, USA), using 150 base-length read chemistry in a paired-end mode.

A Hi-C library was prepared using the Proximo Hi-C Kit. We generated ground tissue for cross-linking using Cryomill (Retsch) and following manufacturer instructions, using a different female than the one used for Nanopore and HiSeq sequencing, from the same natural population. Library construction and sequencing (250 Mio read pairs) was outsourced to Phase Genomics (Seattle).

Assembly pipeline and parameters. Raw Oxford Nanopore reads were filtered using Filtrlong v0.2.0 (<https://github.com/rrwick/Filtrlong>) with the parameters `--min_length 1000 --keep_percent 90 --target_bases 6905000000`. The filtered Nanopore reads were then assembled into contigs using Flye v2.8.1 [26] with `--genome-size 1.3 Gbp`. All Nanopore

reads were mapped against the contigs using minimap2 v2.19 [27] with the parameters `-c -x map-ont` and a first step of polishing was performed using Racon v1.4.3 [28]. Three additional rounds of polishing were then conducted using the Illumina short reads. The short reads were aligned to the contigs using BWA mem v0.7.17 [29] and polishing was performed using Pilon v1.23 [30].

The assembly was decontaminated using BlobTools v1.0 [31] under the taxrule “bestsumorder”. Hit files were generated after a blastn v2.10.1+ against the NCBI nt database, searching for hits with an e-value below $1e-25$ (parameters: `-max_target_seqs 10 -max_hsps 1 -evalue 1e-25`). Contigs without hits to metazoans were removed. Haplotypic duplications were filtered out: filtered reads were mapped against the decontaminated genome using minimap2 and haplotigs were detected with Purge Haplotigs v1.1.1 [32] using the parameters `-l 3 -m 17 -h 190 -j 101` following the recommendations by [32].

For scaffolding, Hi-C reads were mapped to the haploid genome using Juicer v1.6 [33] with the restriction site Sau3AI. Chromosome-level scaffolding was then performed using 3D-DNA v180922 [34] with the parameters `--editor-coarse-resolution 25000`, as recommended by the authors. The resulting Hi-C contact matrices were visualized with Juicebox, and polished following the recommendations by [33]. The completeness of the assembly was assessed with BUSCO v5.1.2 [35] and the *insecta_odb10* dataset using the `--long` and `--augustus` parameters.

To identify the X chromosome in our assembly, we used a coverage approach. We compared coverage between males and females because *Timema* have XX/X0 sex determination [25] and males are expected to show half of the female coverage at the X chromosome. We mapped 3 female (SRS7637462, SRS7637490, and SRS7638308 from [36]) and 4 male samples (PRJNA725673 from [13]) to our scaffolded genome which allowed us to unambiguously identify the third largest scaffold as the X chromosome (S1 Fig).

Gene annotation. The *T. poppense* genome was annotated using a combination of *ab initio* gene prediction, protein homology, and RNA-seq using the Braker2 pipeline v. 2.1.6 [37]. To begin, the genome assembly was soft-masked using RepeatModeler (v. 2.0.2, options: `-LTRStruct, -engine ncbi`) and RepeatMasker (v. 4.1.2, options: `-engine ncbi, -xsmall`). For protein evidence, we used the arthropod protein sequences from OrthoDB v.10.1 [38] and the predicted protein sequences for *Timema* from our previous genome assemblies [36]. For RNAseq evidence, we used our newly generated RNAseq data for *T. poppense* (175 libraries, see below) as well as publicly available RNAseq data from *T. poppense* and the closely related species *T. douglasi* (from [39]) (Bioproject Accessions: PRJNA380865, PRJNA679785, PRJNA1128519) for a total of 376 RNAseq libraries (364 paired-end, 12 single-end) covering 117 different life stages, tissue, and sex combinations. Reads were quality trimmed with Trimmomatic (v. 0.39, options: `ILLUMINACLIP:3:25:6 LEADING:9 TRAILING:9 SLIDINGWINDOW:4:15 MINLEN:80`) [40] before mapping to the genome assembly with STAR (v. 2.7.8a, options: `--twopassMode Basic`) [41]. Braker2 was run using protein evidence and RNAseq separately with the gene predictors Augustus v. 3.4.0 [42] and Genemark v. 4.72 [43]. Following the RNAseq run, UTR predictions were added to the RNAseq gene predictions using GUSHR v. 1.0 [44] in Braker2 (`--addUTR=on`). The separate gene predictions were then merged using TSEBRA v1.0.3 [45] using the `pref_braker1.cfg` configuration file, which weights RNAseq evidence more strongly than the default option. We then ran BUSCO (v. 5.3.2, *insecta_odb10*) on the gene regions annotated by Braker2 and on the whole genome assembly. Any genes found by BUSCO but missed by Braker were then added to the annotation (48 genes). ncRNA genes were predicted using Infernal (v. 1.1.2, minimum e-value $1e-10$) [46]. GO-terms for protein-coding gene predictions were obtained using blastP within OmicsBox v3.1.2, default parameters) to blast the nr *Drosophila melanogaster* database (taxonomy filter: 7227).

Insect husbandry

Hatchlings were obtained from eggs laid by captive bred *T. poppense* individuals, originally collected in California in 2018. To complete development, *Timema* females have one extra molt compared to males [47], hence our aim was to obtain five different tissues (reproductive tracts and four somatic tissues) for each of seven developmental stages in females (nymphal stage 1-6, adult) and six in males (nymphal stage 1-5, adult; [S1 Table](#)). Upon hatching, insects were reared in Petri dishes containing *Ceanothus* plant cuttings wrapped in wet cotton up to a specific developmental stage and then dissected one day after molting. To identify individuals that molted, we painted the thoraxes with red acrylic paint after each molt and checked daily for individuals without the paint. Prior to dissection, the insects were anesthetized with CO₂. Brain, antennae, legs, and gut samples were obtained from each developmental stage ([Fig 1A](#)), while the reproductive tract was collected at every stage from the 4th nymphal stage ([S1 Table](#)). We dissected reproductive tracts only starting from the 4th nymphal stage because we were originally unable to unambiguously identify gonad tissues in the earlier stages. Upon improving our dissection techniques, we were later able to identify and dissect gonad tissues at earlier stages, and we therefore secondarily added reproductive tract samples of newly hatched individuals (1st nymphal stage) ([Fig 1A](#)). During dissections, tissues were placed in Eppendorf tubes and immediately flash frozen in liquid nitrogen before storage at -80°C until extraction for approximately 1/3 of the dissections. For the remaining dissections, due to pandemic-related laboratory closures, tissues were preserved in RNA later (Qiagen) before storage at -80°C. In total, we obtained two to four replicates per sex and tissue ([S1 Table](#)).

RNA extraction and sequencing

TRIzol solution (1 mL) and a small amount of ceramic beads (Sigmund Lindner) were added to each tube containing tissue. Samples were homogenized using a tissue homogenizer (Precellys Evolution; Bertin Technologies). Chloroform (200 µL) was added to each sample and samples were then vortexed for 15 seconds and centrifuged for 25 minutes at 12,000 revolutions per minute (rpm) at 4°C. The upper phase containing the RNA was then transferred to a new 1.5 mL tube with the addition of isopropanol (650 µL) and GlycoBlue Coprecipitant; 1 µL). The samples were vortexed and placed at -20°C overnight. Samples were then centrifuged for 30 minutes at 12,000 rpm at 4°C. The liquid supernatants were removed, and the RNA pellet underwent two washes using 80% and 70% ethanol. Each wash was followed by a 5-minute centrifugation step at 12,000 rpm. Finally, the RNA pellet was resuspended in nuclease-free water and quantified using a fluorescent RNA-binding dye (Quantifluor RNA System) and nanodrop (DS-11 FX).

Library preparation using NEBNext (New England BioLabs) and sequencing on an Illumina NovaSeq 6000 platform with 100 bp paired-end sequencing (~45 million read pairs per sample on average) was outsourced to a sequencing facility (Fasteris, Geneva).

Data analyses

Read counting. Aligned RNA-Seq reads, sorted by genomic position, were processed to count reads mapped to exonic regions using HTseq [48] (v.0.11.2, options: --order=pos --type=exon --idattr=gene_id --stranded=reverse).

Dosage compensation analysis. We categorized the data based on tissue and developmental stage. Subsequently, we excluded genes with low expression, specifically those that were not expressed in a minimum of two libraries and with expression levels lower than 0.5 CPM (counts per million) across samples within the specified tissue and stage. Upon filtering, the number of genes kept for analysis ranged between 12143 and 14424 in different

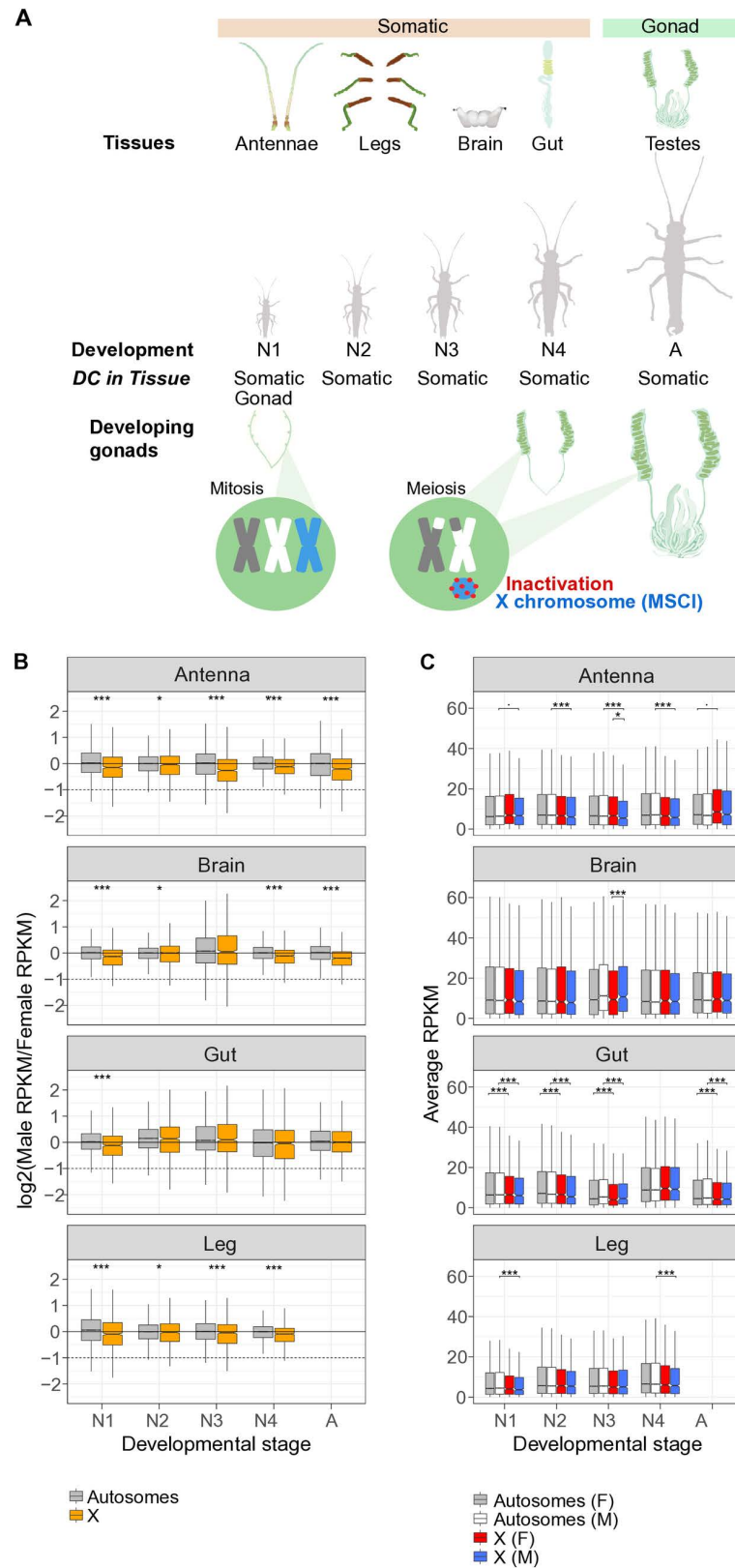


Fig 1. Complete dosage compensation in male somatic tissues during development. A) Schematic overview of male developmental stages in *Timema* stick insects (hemimetabolous development), different analyzed tissues, and

main findings. B) Log₂ of male to female expression ratio for the X (orange) and autosomes (grey) in somatic tissues along development. Dashed lines represent a two-fold reduction in expression in males (as expected if there was no dosage compensation). See [S2 Fig](#) for individual rather than pooled autosomes C) Average expression levels (RPKM values) of genes located on the autosomes and X in females (grey and red) and in males (white and blue) in somatic tissues during development. Boxplots depict the median, the lower and upper quartiles, while the whiskers represent the minimum and maximum values, within 1.5x the interquartile range. See [S3 Fig](#) for individual rather than pooled autosomes. Significance symbols denote: ***= $p < 0.01$, *= $p < 0.05$, = $p = 0.05$.

<https://doi.org/10.1371/journal.pgen.1011615.g001>

tissues and stages. Samples were then normalized for their library sizes using the function “calcNormFactors” in EdgeR [49].

For the computation of RPKM values, we first obtained gene sizes using the Genomic-Features package [50] and then calculated the average RPKM values for each sex using the “rowMeans” function in EdgeR [49]. Lastly, we determined the log₂ RPKM ratio between the male and female average expression levels. Statistical analyses (Wilcoxon tests) and graphical representations of the data were performed in R (4.3.1).

Tissue specificity (Tau). To test if the X chromosome has more tissue-specific expression than the autosomes, we calculated Tau, an index of gene expression tissue specificity ranging from zero (expressed equally in all studied tissues) to one (gene expressed in only one tissue) [51]. For these analyses we used the subset of four tissues (antenna, brain, gut and reproductive tract) and four developmental stages (1st, 3rd, 4th nymphal and the adult stage) for which we had data for both sexes (see [S1 Table](#)). Using median expression RPKM values, we calculated Tau for the 12 longest scaffolds (corresponding to the 12 chromosomes of *T. poppense*). We visualized the results with ggplot2 (v. 3.3.2) [52].

Immunofluorescence staining of male meiotic cells. We assessed X transcriptional activity and heterochromatinization in male meiotic cells via immunofluorescence staining. In order to determine the presence of meiotic cells, we used SMC3_488 (#AB201542, AbCam; hereafter SMC3) as a marker of cohesin axes (this allows for the assessment of synapsis progression, and hence, cell cycle). We performed double immunolabeling of SMC3 with RNA polymerase II phosphorylated at serine 2 (p-RNApol-II-[S2P](#); ab193468, AbCam), an indicator of transcriptional activity, and with H3K9me3 (tri-methylation of histone H3 at lysine-9; #AB8898, AbCam), a histone modification generally associated with heterochromatic silencing, and which marks the silenced X chromosome in male mouse spermatogenesis [53,54]. Gonads from 1st and 4th nymphal stage males were dissected in 1X PBS and fixed in paraformaldehyde (2%) and Triton X-100 (0.1%) solution for 15 minutes. Gonads were then squashed on slides coated with poly-L-lysine, and flash frozen in liquid nitrogen. Slides were incubated in PBS 1x for 20 minutes at room temperature, then blocked with a BSA 3% solution (prepared by dissolving 3g of BSA in 100mL of PBS 1X) for 20 minutes. Slides were then incubated overnight at 4°C in a humid chamber with the primary (p-RNA-Pol II or H3K9me3), diluted in BSA 3% (1:100), and washed 3x for 5 minutes in PBS 1X. The secondary antibody, anti-rabbit Alexa 594 (711-585-152, Jackson), diluted in BSA 3% (1:100), was applied, and samples were incubated for 45 minutes at room temperature. Further washes were conducted as described above, followed by an extended 10-minute wash in PBS 1X, and by blocking using a 5% Normal Rabbit Serum (NRS) solution (X090210-8, Agilent Technology) for 30 minutes at room temperature. Another 5-minute wash in PBS 1x was performed to remove excess blocking solution. Samples were then incubated with the labeled antibody SMC3_488 (#AB201542, AbCam) at a 1:100 dilution for 1 hour at room temperature, followed by a final series of washes and staining with DAPI (D9542, Sigma-Aldrich) for 3 minutes at room temperature. Finally, after a 5-minute wash in 1x PBS, two drops of Vectashield were added to the slide, which was then covered with a coverslip, and

sealed with nail varnish for imaging. Image acquisition was performed at the Cellular Imaging Facility (CIF, University of Lausanne) using a Zeiss LSM 880 Airyscan equipped with a 60x/oil immersion objective. Image processing (cropping and pseudocoloring), was carried out using Fiji [55].

ChIP-sequencing to reveal heterochromatin marks. To profile silencing histone modifications on the X chromosome in male gonads and corroborate that the strongly heterochromatinized chromosome revealed by immunofluorescence staining (see results) was in fact the X chromosome, we conducted ChIP-sequencing using H3K9me3 (based on the same antibody as used for immunofluorescence staining). We dissected male gonads (~ 40 individuals) and immediately froze them in liquid nitrogen. For chromatin preparations, the pooled frozen gonads were homogenized by cryogenic grinding (CryoMill; Retsch GmbH) using a specific regimen (2x 60 s, 25 Hz, resting 30 s, 5 Hz), transferred to a 15-ml Falcon tube, and subsequently subjected to rotation at room temperature for 12 minutes in a cross-linking solution composed of 50 mM Hepes (pH 7.9), 1 mM EDTA (pH 8), 0.5 mM EGTA (pH 8), 100 mM NaCl, and 1% formaldehyde. The cross-linking reaction was stopped by pelleting nuclei for 2 min at 2000g, followed by rotation for 10 minutes in a stop solution containing PBS, 125 mM glycine, and 0.01% Triton X-100. Nuclei were then subjected to washing steps in solution A [10 mM Hepes (pH 7.9), 10 mM EDTA (pH 8), 0.5 mM EGTA (pH 8), and 0.25% Triton X-100] and solution B [10 mM Hepes (pH 7.9), 1 mM EDTA (pH 8), 0.5 mM EGTA (pH 8), 0.01% Triton X-100, and 200 mM NaCl]. This was followed by a sonication step in 100 μ l of radioimmunoprecipitation assay (RIPA) buffer [10 mM tris-HCl (pH 8), 140 mM NaCl, 1 mM EDTA (pH 8), 1% Triton X-100, 0.1% SDS, 0.1% sodium deoxycholate, and 1 \times complete protease inhibitor cocktail] in AFA microtubes in a Covaris S220 sonicator for 5 min with a peak incident power of 140 W, a duty cycle of 5%, and 200 cycles per burst. Sonicated chromatin was centrifuged to pellet insoluble material and snap-frozen.

ChIP was carried out using 5 μ l of H3K9me3 (#AB8898, AbCam) incubated overnight at 4°C with half of the prepared chromatin sample (10 μ l of the same chromatin preparation was used as input control, see below). Protein A Dynabeads (50 μ l; Thermo Fisher Scientific, 100-01D and 100-03D) were added for 3 hours at 4°C, and subsequently washed for 10 min each once with RIPA, four times with RIPA with 500 mM NaCl, once in LiCl buffer [10 mM tris-HCl (pH 8), 250 mM LiCl, 1 mM EDTA, 0.5% IGEPAL CA-630, and 0.5% sodium deoxycholate], and twice in TE buffer [10 mM tris-HCl (pH 8) and 1 mM EDTA]. DNAs of the ChIP sample and the input control were then purified by ribonuclease digestion, proteinase K digestion, reversal of cross-links at 65°C for 6 hours, and elution from a QIAGEN MinElute PCR purification column. The purified DNA (ChIP and input) was then processed at the Lausanne Genomic Technologies Facility for library preparation using the NEBNext Ultra II DNA Library Prep Kit for Illumina and 150-bp paired-end sequencing on an Illumina HiSeq 4000.

ChIP and input reads were trimmed using trimmomatic (v0.39). The reads were then mapped to the reference genome using the BWA-MEM algorithm v0.7.17 (-c 1000000000), with ~57 million reads mapped and with a total mapping efficiency of 99.57%. Chimeric reads were removed using SA:Z tags, and PCR duplicates were eliminated with Picard tools (v2.26.2). Mean coverage was computed for ChIP and input reads within non-overlapping 30 kb windows across all scaffolds using BEDTools (v2.30.0) and normalized by the number of mapped reads in each library. For each genomic window, we computed the log₂ ratio of H3K9me3 ChIP to input coverage. We visualized the data using the ggplot2 package in R (v3.42.4). Smoothing lines were added using a Generalized Additive Model (GAM) to highlight signal strengths across the genome, with smoothing applied individually to each scaffold to visualize differences between chromosomes.

Results and discussion

Complete dosage compensation across male somatic tissues and developmental stages

T. poppense stick insects have 12 chromosomes, comprising one X chromosome (third in size) and 11 autosomes [25]. Our genome assembly fully matches the structure expected from karyotypes, with 1.26 Gbp (94%) of the 1.34 Gbp assembly comprised in the 12 longest scaffolds (hereafter chromosomes) and scaffold 3 corresponding to the X chromosome (132.38 Mbp and harboring ~6% of total genes; S1 Fig). In all four somatic tissues examined (guts, brains, antennae, legs), males feature complete dosage compensation throughout nymphal development as well as at the adult stage. This is revealed by similar ratios of male to female expression for autosomal and X-linked genes (Fig 1B, S2 Table). Additionally, gene expression levels are relatively constant along the single male X (S2 Fig). This indicates that dosage compensation is achieved through a global mechanism that affects the entire chromosome.

While dosage compensation is complete between males and females, sometimes referred as dosage balance [56] (Fig 1B), X-linked genes generally have significantly lower expression than autosomal genes in male somatic tissues (Fig 1C; S3 Table). A similar pattern is observed for females (Fig 1C), with a significant reduction of X-linked expression in female gut and gonad tissue; (S3 Table). It can be argued that complete dosage compensation should refer to situations where the single X is transcribed at a level comparable to the ancestral levels for two X copies, prior to X chromosome formation (i.e., when the X chromosome would have been an autosome; [56]). However, the X chromosome in stick insects has been conserved for at least 120 Mya (within the Phasmatodea order [13,57]) and shares most of its content with the X chromosome in other insect orders that diverged over 450 million years ago [15]. This very deep conservation makes the inference of the ancestral transcription levels challenging.

Independently of the most appropriate terminology, the reduced expression of X-linked as compared to autosomal genes in females might indicate that the mechanism of dosage compensation in stick insects involves downregulation of the X chromosomes in females, similar to *C. elegans*. Alternatively, there may also be a limit to how much the transcriptional activity of the single X in males can be increased. This would favor the movement of highly expressed genes from the X to autosomes [58,59]. A limit to the maximal transcriptional activity of the single X in males is notably believed to explain X chromosome gene content and reduced expression levels in therian mammals [58,59] and *Drosophila* fruit flies [60]. Support for a similar explanation in *Timema* stems from the increased tissue-specificity of X-linked genes in both male and female *Timema* (Wilcoxon test, $p_{\text{adj}}(\text{females}) = 3.5\text{e-}11$, $p_{\text{adj}}(\text{males}) = 2.3\text{e-}08$; Fig 2; see also S4 Fig and S5 Table). This mirrors findings in mammals where tissue-specific genes are generally less highly expressed than broadly expressed genes [59,61], although opposite patterns are reported in *Drosophila* [62,63]. However, it is important to note that dosage compensation is a feature of individual cells and that a greater expression breadth across tissues does not necessarily equate with a higher expression level within individual cells, as would be the case if there was high heterogeneity in expression among cells within a tissue.

Additionally, X chromosome degradation could also contribute to lower expression of X-linked as compared to autosomal genes, similar to patterns reported for genes on the Y chromosomes in some species [64]. The X chromosome has a reduced effective population size as compared to autosomes, as a consequence of reduced copy numbers and the lack of X recombination in males, which leads to the accumulation of deleterious mutations in *Timema* [13].

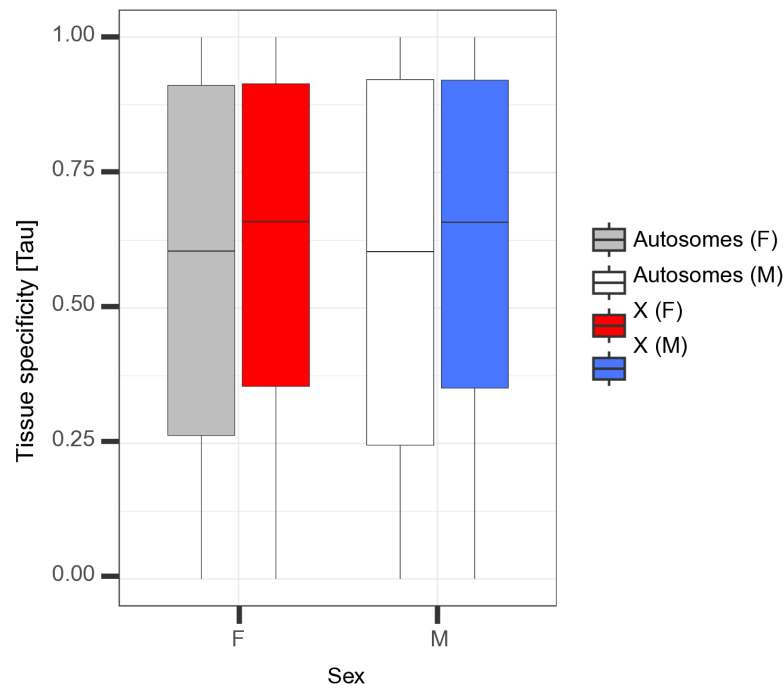


Fig 2. X-linked genes are more tissue-specific in their expression than autosomal genes. Tissue specificity of expression for genes on the X chromosome in males (blue box) and females (red box), compared to autosomal genes (white and gray boxes), calculated across four tissues. Boxes depict the median, the lower and upper quartiles, while the whiskers represent the minimum and maximum values, within 1.5x the interquartile range. Note that this pattern is not solely driven by averaging values across 11 autosomes or gene expression in gonads (S4 Fig).

<https://doi.org/10.1371/journal.pgen.1011615.g002>

Early presence and later absence of dosage compensation in the male reproductive tract

The patterns of X-linked expression in *Timema* male reproductive tracts differ strikingly from those observed in somatic tissues. During the first nymphal stage, there is complete dosage compensation in the reproductive tract, similar to somatic tissues (Fig 3A–3C, and S4 Fig). However, from the 4th nymphal stage, there is a strong reduction of X-linked expression in males, relatively constant along the length of the X (S6 Fig), and which persists throughout development and until the adult stage (Fig 3). We first hypothesized that dosage compensation might be active during early gonad development in the first nymphal stage because the tissue was not yet strongly sexually differentiated. However, this is not the case as the degree of gonadal sexual differentiation (as measured from sex biased gene expression) is relatively constant throughout development. Already 44% of the expressed genes in gonads show sex-biased expression at the first nymphal stage, as compared to 45% at the 4th nymphal stage or 53% in adults (S4 Table).

Next, we evaluated whether the strong reduction of X-linked expression from the 4th nymphal stage was caused by meiotic X-chromosome inactivation, as is well described in therian mammals [65]. Indeed, the extent of the reduction significantly exceeds the two-fold reduction expected in the absence of dosage compensation (Wilcoxon signed rank test with continuity correction; 4th nymphal stage: $V = 77366$, $p\text{-value} < 2.2e-16$, adult stage: $V = 150046$, $p\text{-value} < 2.2e-16$) indicating other mechanisms are affecting the expression of X linked genes in male gonads (Fig 3A and 3B). Immunostaining of gonad tissue from adult and 4th nymphal stage males corroborates the transcriptional inactivity of the X chromosome. The X

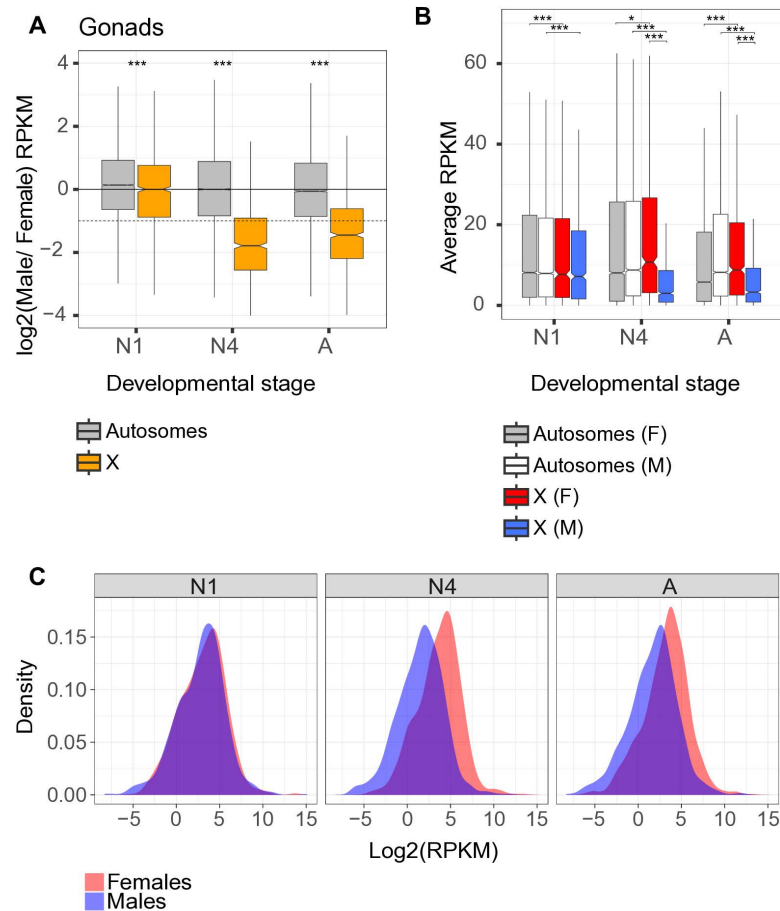


Fig 3. Presence of dosage compensation only during the 1st nymphal stage in male reproductive tracts. A) Log₂ of male to female expression ratio for the X chromosome (orange) and autosomes (gray) at three developmental stages (N1- 1st nymphal, N4- 4th nymphal and A- adult stage) in the reproductive tract. See S5 Fig for individual rather than pooled autosomes. B) Average expression levels (RPKM values) of genes located on the autosomes and X in females (gray and red boxes) and in males (white and blue) at three developmental stages. Boxplots depict the median, the lower and upper quartiles, while the whiskers represent the minimum and maximum values, within 1.5x the interquartile range. See S5 Fig for individual rather than pooled autosomes. C) Distribution of expression levels for X-linked genes in males (blue) and females (red) (overlapping ranges are indicated in purple). Significance symbols denote: ***= $p < 0.01$, * = $p < 0.05$.

<https://doi.org/10.1371/journal.pgen.1011615.g003>

chromosome in male meiotic cells is visible in DAPI staining as highly condensed (“heteropycnotic”; Fig 4), similar to other insects [66]. It also lacks a Pan Phospho RNAPol-II signal, a marker for transcriptional activity, in otherwise transcriptionally active cells (Fig 4). We then also performed immunostaining of meiotic cells for silencing histone modifications (using an H3K9me3 antibody) and profiled the corresponding molecular marks in the genome using ChIP-seq based on male gonad tissue. As expected, the X has a strong H3K9me3 signal (Fig 5A and 5B) and the corresponding H3K9me3 marks are enriched all along the male X (Fig 5C), suggesting that the silencing of the X is achieved via histone modifications (Fig 5).

The patterns of MSCI in stick insects share many parallels with MSCI in mammals and birds [67] but differ strikingly from meiotic X chromosome regulation in the more closely related fly species *D. melanogaster*. Indeed, whether there is some form of targeted X chromosome downregulation in male meiotic cells in *D. melanogaster* is a matter of ongoing debate, although it has become clear that MSCI as known for mammals and now stick insects does

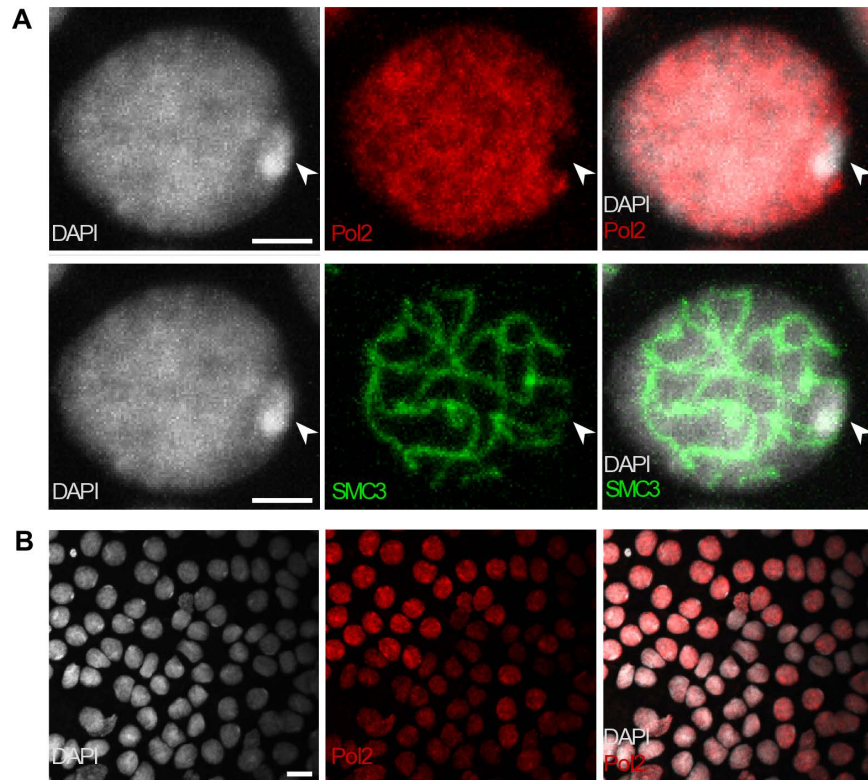


Fig 4. No transcriptional activity of the X chromosome during male meiosis. DAPI, Phospho *S2* RNA Pol-II (Pol2-*S2P*), and SMC3 stainings were applied to germ cell squashes from 4th nymphal stage males, shown as an overlay of multiple focal planes. A) Shown is a cell at the pachytene stage of meiosis I for illustration. The arrow in each image indicates the location of the X chromosome (heteropycnotic body). The Phospho *S2* RNA Pol-II staining highlights phosphorylated forms of RNA polymerase II, indicating regions of transcriptional activity. Scale bar indicates 5µm. B) Zoom out to illustrate the widespread transcriptional activity in meiotic cells and systematic lack of activity on the X chromosome. Scale bar indicates 20µm.

<https://doi.org/10.1371/journal.pgen.1011615.g004>

not occur in *D. melanogaster*. This is revealed by transcriptional profiling of *D. melanogaster* testis [68–70], similar RNA polymerase activity on the X and autosomes [71], and lack of enrichment of silencing histone modifications on the X in the male germline [71].

The difference between stick insects and *Drosophila* regarding X chromosome regulation in male germ cells is interesting because it can help elucidate the reasons for why MSCI evolved and was then secondarily lost or highly modified in a subset of species. Indeed, a possible explanation for MSCI is that it evolved to protect un-synapsed chromosomes (including the X in males) from damaging effects such as ectopic exchanges, non-homologous recombination, and unrepaired double-strand breaks [72]. The tight condensation of the X under MSCI would then shelter the unsynapsed X from such effects. A key difference between male meiosis in *Timema* stick insects and *D. melanogaster* is that meiosis is achiasmatic in *Drosophila* males [73] but chiasmatic in *Timema* [13]. The evolution of a completely achiasmatic meiosis in *Drosophila* males means that all chromosomes, not only hemizygous sex chromosomes, would be exposed to damaging effects in the absence of synapsis. Such a situation should generate strong selection for sheltering mechanisms not linked to hemizygoty [72] and could thus explain the loss of classical MSCI.

An association between achiasmasy and lack of classical MSCI via strong X condensation is supported beyond the *Timema* vs *Drosophila* dichotomy by a survey of older cytogenetic

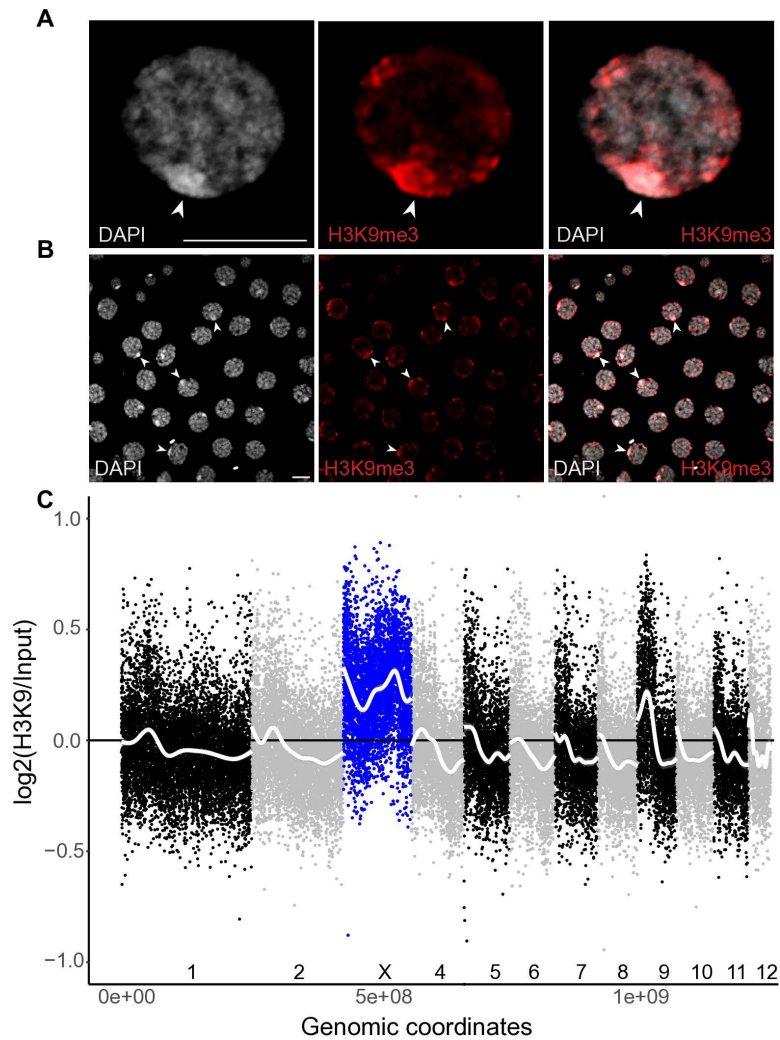


Fig 5. Enrichment of the H3K9me marks on the X chromosome in adult male testes. A, B) DAPI (blue) and H3K9me3 (magenta) applied to cells from male adult gonad squashes. Images from a single focal plane, of one individual A) single germ cell at pachytene stage, with X indicating the location of the X chromosome (scale bar 10 μ m) B) Many germ cells, with arrows pointing to the X chromosome C) Log₂ ratio of H3K9me to input ChIP-Seq data along the genome, 30K window size. The X chromosome is depicted in blue, while autosomes are depicted in black or gray, and chromosome number (1-12) is further indicated above the Y axis. Smoothing lines (method “gam”) for each scaffold are in white.

<https://doi.org/10.1371/journal.pgen.1011615.g005>

data in insects. Chiasmatic insects, including most species in the orders Orthoptera, Blattodea, Mantodea and the suborder Heteroptera, typically show sex chromosome morphologies that likely reflect heterochromatization (i.e., MSCI), while many (though not all) achiasmatic insects do not. This pattern is consistent with the idea that achiasmatic insects evolved from ancestral, chiasmatic forms with MSCI; some achiasmatic groups have then subsequently lost MSCI [72].

Independently of the causes underlying the evolution and loss of MSCI, the contrasting X-expression patterns in male reproductive tracts of hatchlings versus 4th nymphal stage likely reflect the start of meiosis I. Thus, in hatchlings where dosage compensation is complete (Fig 3A), cell divisions would be largely mitotic (spermatogonia stage). MSCI would start in cells entering meiosis I, resulting in the X-linked expression pattern we observe in reproductive

tracts at the 4th nymphal stage (Fig 3A). In accordance with these interpretations, observation of cells from 4th nymphal stage testes reveal the presence of many cells at meiosis I, whereas we could not find a single cell in meiosis I in squashes from testes of male hatchlings (S7 Fig). Finally, it appears that X-linked expression is somewhat elevated in reproductive tracts of adult males as compared to those of 4th nymphal stage males (Fig 3A). This is most likely due to the larger portion of somatic tissues in adult male reproductive tracts, most notably accessory glands, which are very small in all nymphal stages but well developed in adults (Jelisaveta Djordjevic, personal observation, see Fig 1A). Such a pattern is known to also occur in *Caenorhabditis elegans*, where the X is completely silenced in germ cells and changes in X-linked expression during development are caused by changes in the ratio of somatic to germ cells [56,74,75]. More generally, the observation of reduced X-expression in male gonads without investigation of associated mechanism is typically interpreted as lack of dosage compensation in this tissue [11–13,56]. However, as we observe in *Timema*, dosage compensation in males may well be ubiquitous across tissues and developmental stages in many species, and reduced X-expression patterns would solely be driven by MSCI.

Conclusion

Dosage compensation by upregulation of the single X in males consistently occurs in somatic tissues across development in *Timema poppense*. By contrast, X-expression in male reproductive tracts is dynamic. It starts with complete dosage compensation in the first nymphal stage, when spermatogonia have not yet entered meiosis I, and is followed by X inactivation in later nymphal stages when most gonadal cells are undergoing meiotic divisions. We suggest that the reduced X-linked expression in testes is solely driven by X chromosome inactivation during meiosis, and does not stem from a lack of dosage compensation in *Timema*. This is likely generally the case in insects with reduced X-linked expression in testes.

Supporting information

S1 Table. Number of RNA-seq samples per sex, for every developmental stage and tissue. (XLSX)

S2 Table. Results of Wilcoxon tests where the ratio of male to female average RPKM values were compared between autosomes and the X chromosome within every developmental stage and tissue. The column “stage” indicates the developmental stage; N1–N4 (1st to 4th nymphal stage), A- adult, the column “tissue” the different tissues, the column; “p.adjusted”- fdr correction of p-values for multiple testing using the Benjamini & Hochberg method (Benjamini and Hochberg 1995). (XLSX)

S3 Table. Results of Wilcoxon tests where average RPKM values were compared for autosomal and X-linked genes for each sex and within each developmental stage and tissue (indicated in the “Tissue” column). The “Stage” column denotes the developmental stage, with N1–N4 representing the 1st to 4th nymphal stages and A indicating the adult stage. **Columns: Group1 and Group2:** Specify the groups being compared, with colored cells highlighting the comparisons of interest. **“p.adjusted”:** Represents the false discovery rate (FDR) corrected p-values, utilizing the Benjamini & Hochberg method for multiple testing. (XLSX)

S4 Table. Sex-biased gene counts during reproductive tract development at N1 (1st nymphal), N4 (4th nymphal), and A (adult) stages. It includes MB (male-biased), FB

(female-biased), SB (total sex-biased genes), and T (total expressed genes) categories, with percentages in brackets. Differential gene expression between the sexes was assessed using a generalized linear model with a quasi-likelihood F-test (Chen, et al. 2016) in edgeR v.3.42.4 (Robinson, et al. 2009; McCarthy, et al. 2012) in each of the three developmental stages as described in (Djordjevic, et al. 2022).

(XLSX)

S5 Table. Wilcoxon tests comparing tissue specificity [Tau], calculated across three somatic tissues, between scaffolds within each sex (“variable”; Females, Males). Columns: Group1 and Group2: Specify the scaffolds being compared, with colored cells highlighting the comparisons of interest, **“p.adjusted”:** Represents the false discovery rate (FDR) corrected p-values, utilizing the Benjamini & Hochberg method for multiple testing.

(XLSX)

S1 Fig. *T. poppense* X chromosome identification. The plot shows the \log_2 ratio of male to female coverage of 100 kb sliding windows across the genome. Alternated colours designate different chromosomes, with chromosome 3 showing a much lower overall male to female coverage ratio.

(TIF)

S2 Fig. Mean expression levels per gene along the X chromosome (in base pairs) in brain somatic tissue at 1st (N1), 4th (N4) and adult (A) stages in females (left) and males (right). The line in each panel represents a loess (Locally Estimated Scatterplot Smoothing) smoothed curve, a non-parametric regression method that fits localized linear regressions to subsets of the data, highlighting overall expression patterns along chromosome.

(TIF)

S3 Fig. Log2 of male to female expression ratio across all 12 *T. poppense* chromosomes at five developmental stages: N1, N2, N3, N4, and A (representing the 1st to 4th nymphal stages and the adult stage, respectively). Chromosome 3, represented in orange, corresponds to the X chromosome, while autosomes are depicted in gray. The panels, arranged from top to bottom, showcase the Log2 ratio in different somatic tissues: antenna, brain, guts, and legs. Boxplots depict the median, the lower and upper quartiles, while the whiskers represent the minimum and maximum values, within 1.5x the interquartile range.

(TIF)

S4 Fig. A) Average RPKM expression levels across chromosomes in females (grey) and in males (white) along development, chromosome three corresponds to the X and is depicted in red (females) and blue (males). The panels, from top to bottom, showcase the Average RPKM in different somatic tissues: antenna, brain, guts, and legs. Boxplots depict the median, the lower and upper quartiles, while the whiskers represent the minimum and maximum values, within 1.5x the interquartile range. B) Distribution of expression levels for X-linked genes in males (blue) and females (red) (overlapping ranges are indicated in purple) across developmental stages and somatic tissues.

(TIF)

S5 Fig. A) Tissue specificity of X chromosomes in males (M) (blue box) and females (F) (red box) as compared to the autosomes (white and gray boxes), calculated across three somatic tissues. Because genes on the X are often testes or ovaries specific, we here repeated the analysis presented in the main text based on four tissues (three somatic tissues and reproductive tracts) with the three somatic tissues only, and X tissue specificity remained higher than autosomes Wilcoxon test, $p_{\text{adj (females)}} = 6.7\text{e-}13$, $p_{\text{adj (males)}} = 2.4\text{e-}16$ B) Tissue specificity in

females (F) and males (M) across scaffolds (see [S5 Table](#)), based on three somatic tissues. Scaffold 3, represented in orange, corresponds to the X chromosome, while other scaffolds are depicted in gray. Boxplots depict the median, the lower and upper quartiles, while the whiskers represent the minimum and maximum values, within 1.5x the interquartile range. (TIF)

S6 Fig. A) The Log₂ ratio of RPKM levels of expression between males and females across scaffolds at three developmental stages (N1, N4, and Adult) in the reproductive tract.

Chromosome three, represented in orange, corresponds to the X chromosome, while other chromosomes are depicted in gray. B) Average RPKM expression levels at three developmental stages (N1, N4, and adult) in the reproductive tract separated for different chromosomes in females (grey) and in males (white) boxes, chromosome three corresponds to the X and is depicted in red (females) and blue (males). Boxplots depict the median, the lower and upper quartiles, while the whiskers represent the minimum and maximum values, within 1.5x the interquartile range.

(TIF)

S7 Fig. Mean expression RPKM levels per gene along the X chromosome at 1st (N1), 4th (N4) and Adult (A) stages in reproductive tracts of females (left) and males (right) panels.

The red line in each panel shows the loess smoothed curve.

(TIF)

S8 Fig. DAPI, SMC3 staining applied to testes squashes of 1st (N1) and 4th (N4) nymphal stage males. SMC3 is a protein of the cohesin complex marking chromosome axes during meiosis I. No cells in meiosis I were detected at N1 (scale bar 10 μ m), while numerous cells at this stage were detected at N4 (scale bar 20 μ m).

(TIF)

Acknowledgments

We thank Corinne Peter and the Lausanne GTF platform for help with ChIP-seq, Bart Zijlstra, Armand Yazdani, Susana Freitas, and Chloé Larose for help in the field, and current and previous members of the Schwander lab for discussions.

Author contributions

Conceptualization: Jelisaveta Djordjevic, Tanja Schwander.

Data curation: Jelisaveta Djordjevic, Jean-Marc Aury, Darren J. Parker.

Formal analysis: Jelisaveta Djordjevic, Patrick Tran Van, Darren J. Parker.

Funding acquisition: Tanja Schwander.

Investigation: Jelisaveta Djordjevic, William Toubiana, Marjorie Labédan, Zoé Dumas, Corinne Cruaud, Karine Labadie.

Methodology: Jelisaveta Djordjevic, Jean-Marc Aury, Benjamin Istace, Benjamin Noel, Tanja Schwander.

Project administration: Tanja Schwander.

Supervision: Tanja Schwander.

Validation: Tanja Schwander.

Visualization: Jelisaveta Djordjevic.

Writing – original draft: Jelisaveta Djordjevic, Tanja Schwander.

Writing – review & editing: Jelisaveta Djordjevic, William Toubiana, Zoé Dumas, Darren J. Parker, Tanja Schwander.

References

1. Stinglee S, Stoehr G, Peplowska K, Cox J, Mann M, Storchova Z. Global analysis of genome, transcriptome and proteome reveals the response to aneuploidy in human cells. *Mol Syst Biol*. 2012;8:608. <https://doi.org/10.1038/msb.2012.40> PMID: [22968442](https://pubmed.ncbi.nlm.nih.gov/22968442/)
2. Ohno S. Sex chromosomes and sex-linked genes. Verlag: Springer; 1967.
3. Straub T, Becker PB. Dosage compensation: the beginning and end of generalization. *Nat Rev Genet*. 2007;8(1):47–57. <https://doi.org/10.1038/nrg2013> PMID: [17173057](https://pubmed.ncbi.nlm.nih.gov/17173057/)
4. Mank JE. Sex chromosome dosage compensation: definitely not for everyone. *Trends Genet*. 2013;29(12):677–83. <https://doi.org/10.1016/j.tig.2013.07.005> PMID: [23953923](https://pubmed.ncbi.nlm.nih.gov/23953923/)
5. Gupta V, Parisi M, Sturgill D, Nuttall R, Doctolero M, Dudko OK, et al. Global analysis of X-chromosome dosage compensation. *J Biol*. 2006;5(1):3. <https://doi.org/10.1186/jbiol30> PMID: [16507155](https://pubmed.ncbi.nlm.nih.gov/16507155/)
6. Nguyen DK, Disteché CM. Dosage compensation of the active X chromosome in mammals. *Nat Genet*. 2006;38(1):47–53. <https://doi.org/10.1038/ng1705> PMID: [16341221](https://pubmed.ncbi.nlm.nih.gov/16341221/)
7. Lyon MF. Gene action in the X-chromosome of the mouse (*Mus musculus* L.). *Nature*. 1961;190:372–3. <https://doi.org/10.1038/190372a0> PMID: [13764598](https://pubmed.ncbi.nlm.nih.gov/13764598/)
8. Meyer BJ, Casson LP. *Caenorhabditis elegans* compensates for the difference in X chromosome dosage between the sexes by regulating transcript levels. *Cell*. 1986;47(6):871–81. [https://doi.org/10.1016/0092-8674\(86\)90802-0](https://doi.org/10.1016/0092-8674(86)90802-0) PMID: [3779843](https://pubmed.ncbi.nlm.nih.gov/3779843/)
9. Meyer B, McDonel P, Csankovszki G, Ralston E, editors. Sex and X-chromosome-wide repression in *Caenorhabditis elegans*. Cold Spring Harbor symposia on quantitative biology; 2004: Cold Spring Harbor Laboratory Press.
10. Lucchesi JC. Dosage compensation in flies and worms: the ups and downs of X-chromosome regulation. *Curr Opin Genet Dev*. 1998;8(2):179–84. [https://doi.org/10.1016/s0959-437x\(98\)80139-1](https://doi.org/10.1016/s0959-437x(98)80139-1) PMID: [9610408](https://pubmed.ncbi.nlm.nih.gov/9610408/)
11. Vicoso B, Bachtrog D. Numerous transitions of sex chromosomes in Diptera. *PLoS Biol*. 2015;13(4):e1002078. <https://doi.org/10.1371/journal.pbio.1002078> PMID: [25879221](https://pubmed.ncbi.nlm.nih.gov/25879221/)
12. Hu Q-L, Ye Y-X, Zhuo J-C, Huang H-J, Li J-M, Zhang C-X. Chromosome-level Assembly, Dosage Compensation and Sex-biased Gene Expression in the Small Brown Planthopper, *Laodelphax striatellus*. *Genome Biol Evol*. 2022;14(11):evac160. <https://doi.org/10.1093/gbe/evac160> PMID: [36317697](https://pubmed.ncbi.nlm.nih.gov/36317697/)
13. Parker DJ, Jaron KS, Dumas Z, Robinson-Rechavi M, Schwander T. X chromosomes show relaxed selection and complete somatic dosage compensation across *Timema* stick insect species. *J Evol Biol*. 2022;35(12):1734–50. <https://doi.org/10.1111/jeb.14075> PMID: [35933721](https://pubmed.ncbi.nlm.nih.gov/35933721/)
14. Blackmon H, Ross L, Bachtrog D. Sex Determination, Sex Chromosomes, and Karyotype Evolution in Insects. *J Hered*. 2017;108(1):78–93. <https://doi.org/10.1093/jhered/esw047> PMID: [27543823](https://pubmed.ncbi.nlm.nih.gov/27543823/)
15. Touns MA, Vicoso B. The X chromosome of insects predates the origin of Class Insecta. *bioRxiv*. 2023:2023.04.19.537501. <https://doi.org/10.1101/2023.04.19.537501>
16. Lucchesi JC, Kuroda MI. Dosage compensation in *Drosophila*. *Cold Spring Harb Perspect Biol*. 2015;7(5):a019398. <https://doi.org/10.1101/cshperspect.a019398> PMID: [25934013](https://pubmed.ncbi.nlm.nih.gov/25934013/)
17. Pal A, Vicoso B. The X Chromosome of Hemipteran Insects: Conservation, Dosage Compensation and Sex-Biased Expression. *Genome Biol Evol*. 2015;7(12):3259–68. <https://doi.org/10.1093/gbe/evv215> PMID: [26556591](https://pubmed.ncbi.nlm.nih.gov/26556591/)
18. Li X, Mank J, Ban L. Grasshopper genome reveals long-term conservation of the X chromosome and temporal variation in X chromosome evolution. *BioRxiv*. 2022:2022.09.08.507201. <https://doi.org/10.1101/2022.09.08.507201>
19. Kalita AI, Marois E, Kozielska M, Weissing FJ, Jaouen E, Möckel MM, et al. The sex-specific factor SOA controls dosage compensation in *Anopheles* mosquitoes. *Nature*. 2023;623(7985):175–82. <https://doi.org/10.1038/s41586-023-06641-0> PMID: [37769784](https://pubmed.ncbi.nlm.nih.gov/37769784/)
20. Krzywinska E, Ribeca P, Ferretti L, Hammond A, Krzywinski J. A novel factor modulating X chromosome dosage compensation in *Anopheles*. *Curr Biol*. 2023;33(21):4697-4703.e4. <https://doi.org/10.1016/j.cub.2023.09.001> PMID: [3774706](https://pubmed.ncbi.nlm.nih.gov/3774706/)
21. Rayner JG, Hitchcock TJ, Bailey NW. Variable dosage compensation is associated with female consequences of an X-linked, male-beneficial mutation. *Proc Biol Sci*. 2021;288(1947):20210355. <https://doi.org/10.1098/rspb.2021.0355> PMID: [33757350](https://pubmed.ncbi.nlm.nih.gov/33757350/)

22. Turner JMA. Meiotic sex chromosome inactivation. *Development*. 2007;134(10):1823–31. <https://doi.org/10.1242/dev.000018> PMID: 17329371
23. Namekawa SH, Lee JT. XY and ZW: is meiotic sex chromosome inactivation the rule in evolution?. *PLoS Genet*. 2009;5(5):e1000493. <https://doi.org/10.1371/journal.pgen.1000493> PMID: 19461890
24. Kramer M, Kranz A-L, Su A, Winterkorn LH, Albritton SE, Ercan S. Developmental Dynamics of X-Chromosome Dosage Compensation by the DCC and H4K20me1 in *C. elegans*. *PLoS Genet*. 2015;11(12):e1005698. <https://doi.org/10.1371/journal.pgen.1005698> PMID: 26641248
25. Schwander T, Crespi BJ. Multiple direct transitions from sexual reproduction to apomictic parthenogenesis in *Timema* stick insects. *Evolution*. 2009;63(1):84–103. <https://doi.org/10.1111/j.1558-5646.2008.00524.x> PMID: 18803687
26. Kolmogorov M, Yuan J, Lin Y, Pevzner PA. Assembly of long, error-prone reads using repeat graphs. *Nat Biotechnol*. 2019;37(5):540–6. <https://doi.org/10.1038/s41587-019-0072-8> PMID: 30936562
27. Li H. Minimap2: pairwise alignment for nucleotide sequences. *Bioinformatics*. 2018;34(18):3094–100. <https://doi.org/10.1093/bioinformatics/bty191> PMID: 29750242
28. Vaser R, Sović I, Nagarajan N, Šikić M. Fast and accurate de novo genome assembly from long uncorrected reads. *Genome Res*. 2017;27(5):737–46. <https://doi.org/10.1101/gr.214270.116> PMID: 28100585
29. Li H. Aligning sequence reads, clone sequences and assembly contigs with BWA-MEM. arXiv preprint arXiv:13033997. 2013. <https://doi.org/arXiv:13033997>
30. Walker BJ, Abeel T, Shea T, Priest M, Abouelliel A, Sakthikumar S, et al. Pilon: an integrated tool for comprehensive microbial variant detection and genome assembly improvement. *PLoS One*. 2014;9(11):e112963. <https://doi.org/10.1371/journal.pone.0112963> PMID: 25409509
31. Laetsch DR, Blaxter ML. BlobTools: Interrogation of genome assemblies. *F1000Res*. 2017;6:1287. <https://doi.org/10.12688/f1000research.12232.1>
32. Roach MJ, Schmidt SA, Borneman AR. Purge Haplotigs: allelic contig reassignment for third-gen diploid genome assemblies. *BMC Bioinformatics*. 2018;19(1):460. <https://doi.org/10.1186/s12859-018-2485-7> PMID: 30497373
33. Durand NC, Shamim MS, Machol I, Rao SSP, Huntley MH, Lander ES, et al. Juicer Provides a One-Click System for Analyzing Loop-Resolution Hi-C Experiments. *Cell Syst*. 2016;3(1):95–8. <https://doi.org/10.1016/j.cels.2016.07.002> PMID: 27467249
34. Dudchenko O, Batra SS, Omer AD, Nyquist SK, Hoeger M, Durand NC, et al. De novo assembly of the *Aedes aegypti* genome using Hi-C yields chromosome-length scaffolds. *Science*. 2017;356(6333):92–5. <https://doi.org/10.1126/science.aal3327> PMID: 28336562
35. Seppey M, Manni M, Zdobnov E. BUSCO: assessing genome assembly and annotation completeness. *Gene prediction: methods and protocols*. 2019:227–45.
36. Jaron KS, Parker DJ, Anselmetti Y, Tran Van P, Bast J, Dumas Z, et al. Convergent consequences of parthenogenesis on stick insect genomes. *Sci Adv*. 2022;8(8):eabg3842. <https://doi.org/10.1126/sciadv.abg3842> PMID: 35196080
37. Brůna T, Hoff KJ, Lomsadze A, Stanke M, Borodovsky M. BRAKER2: automatic eukaryotic genome annotation with GeneMark-EP+ and AUGUSTUS supported by a protein database. *NAR Genom Bioinform*. 2021;3(1):lqaa108. <https://doi.org/10.1093/nargab/lqaa108> PMID: 33575650
38. Kriventseva EV, Kuznetsov D, Tegenfeldt F, Manni M, Dias R, Simão FA, et al. OrthoDB v10: sampling the diversity of animal, plant, fungal, protist, bacterial and viral genomes for evolutionary and functional annotations of orthologs. *Nucleic Acids Res*. 2019;47(D1):D807–11. <https://doi.org/10.1093/nar/gky1053> PMID: 30395283
39. Toubiana W, Dumas Z, Van PT, Parker DJ, Mérel V, Schubert V, et al. Functional monocentricity with holocentric characteristics and chromosome-specific centromeres in a stick insect. *Sci Adv*. 2025;11(1):eads6459. <https://doi.org/10.1126/sciadv.ads6459> PMID: 39742490
40. Bolger AM, Lohse M, Usadel B. Trimmomatic: a flexible trimmer for Illumina sequence data. *Bioinformatics*. 2014;30(15):2114–20. <https://doi.org/10.1093/bioinformatics/btu170> PMID: 24695404
41. Dobin A, Davis CA, Schlesinger F, Drenkow J, Zaleski C, Jha S, et al. STAR: ultrafast universal RNA-seq aligner. *Bioinformatics*. 2013;29(1):15–21. <https://doi.org/10.1093/bioinformatics/bts635> PMID: 23104886
42. Stanke M, Keller O, Gunduz I, Hayes A, Waack S, Morgenstern B. AUGUSTUS: ab initio prediction of alternative transcripts. *Nucleic Acids Res*. 2006;34(Web Server issue):W435–9. <https://doi.org/10.1093/nar/gkl200> PMID: 16845043
43. Brůna T, Lomsadze A, Borodovsky M. GeneMark-EP+: eukaryotic gene prediction with self-training in the space of genes and proteins. *NAR Genom Bioinform*. 2020;2(2):lqaa026. <https://doi.org/10.1093/nargab/lqaa026> PMID: 32440658

44. Keilwagen J, Hartung F, Grau J. GeMoMa: homology-based gene prediction utilizing intron position conservation and RNA-seq data. *Gene prediction: Methods and protocols*. 2019;161–77.
45. Gabriel L, Hoff KJ, Brůna T, Borodovsky M, Stanke M. TSEBRA: transcript selector for BRAKER. *BMC Bioinformatics*. 2021;22(1):566. <https://doi.org/10.1186/s12859-021-04482-0> PMID: 34823473
46. Nawrocki E, Eddy S. Infernal 1.1: 100-fold faster RNA homology searches. *Bioinformatics*. 2013;29(22):2933–5.
47. Djordjevic J, Dumas Z, Robinson-Rechavi M, Schwander T, Parker DJ. Dynamics of sex-biased gene expression during development in the stick insect *Timema californicum*. *Heredity*. 2022;1–10.
48. Anders S, Pyl PT, Huber W. HTSeq—a Python framework to work with high-throughput sequencing data. *Bioinformatics*. 2015;31(2):166–9. <https://doi.org/10.1093/bioinformatics/btu638> PMID: 25260700
49. Robinson MD, McCarthy DJ, Smyth GK. edgeR: a Bioconductor package for differential expression analysis of digital gene expression data. *Bioinformatics*. 2010;26(1):139–40. <https://doi.org/10.1093/bioinformatics/btp616> PMID: 19910308
50. Lawrence M, Huber W, Pagès H, Aboyoun P, Carlson M, Gentleman R, et al. Software for computing and annotating genomic ranges. *PLoS Comput Biol*. 2013;9(8):e1003118. <https://doi.org/10.1371/journal.pcbi.1003118> PMID: 23950696
51. Yanai I, Benjamin H, Shmoish M, Chalifa-Caspi V, Shklar M, Ophir R, et al. Genome-wide midrange transcription profiles reveal expression level relationships in human tissue specification. *Bioinformatics*. 2005;21(5):650–9. <https://doi.org/10.1093/bioinformatics/bti042> PMID: 15388519
52. Wickham H. ggplot2: Elegant graphics for data analysis. Springer-Verlag New York; 2016.
53. Khalil AM. Histone modifications and chromatin dynamics of the mammalian inactive sex chromosomes. University of Florida; 2004.
54. Ernst C, Eling N, Martinez-Jimenez CP, Marioni JC, Odom DT. Staged developmental mapping and X chromosome transcriptional dynamics during mouse spermatogenesis. *Nat Commun*. 2019;10(1):1251. <https://doi.org/10.1038/s41467-019-09182-1> PMID: 30890697
55. Schindelin J, Arganda-Carreras I, Frise E, Kaynig V, Longair M, Pietzsch T, et al. Fiji: an open-source platform for biological-image analysis. *Nat Methods*. 2012;9(7):676–82. <https://doi.org/10.1038/nmeth.2019> PMID: 22743772
56. Gu L, Walters JR. Evolution of Sex Chromosome Dosage Compensation in Animals: A Beautiful Theory, Undermined by Facts and Bedeviled by Details. *Genome Biol Evol*. 2017;9(9):2461–76. <https://doi.org/10.1093/gbe/evx154> PMID: 28961969
57. Stuart OP, Cleave R, Magrath MJL, Mikheyev AS. Genome of the Lord Howe Island Stick Insect Reveals a Highly Conserved Phasmid X Chromosome. *Genome Biol Evol*. 2023;15(6):evad104. <https://doi.org/10.1093/gbe/evad104> PMID: 37279506
58. Vicoso B, Charlesworth B. Effective population size and the faster-X effect: an extended model. *Evolution*. 2009;63(9):2413–26. <https://doi.org/10.1111/j.1558-5646.2009.00719.x> PMID: 19473388
59. Hurst LD, Ghanbarian AT, Forrest ARR, FANTOM consortium, Huminiecki L. The Constrained Maximal Expression Level Owing to Haploidy Shapes Gene Content on the Mammalian X Chromosome. *PLoS Biol*. 2015;13(12):e1002315. <https://doi.org/10.1371/journal.pbio.1002315> PMID: 26685068
60. Argyridou E, Parsch J. Regulation of the X Chromosome in the Germline and Soma of *Drosophila melanogaster* Males. *Genes (Basel)*. 2018;9(5):242. <https://doi.org/10.3390/genes9050242> PMID: 29734690
61. Pessia E, Engelstädter J, Marais GAB. The evolution of X chromosome inactivation in mammals: the demise of Ohno's hypothesis?. *Cell Mol Life Sci*. 2014;71(8):1383–94. <https://doi.org/10.1007/s00018-013-1499-6> PMID: 24173285
62. Mikhaylova LM, Nurminsky DI. Lack of global meiotic sex chromosome inactivation, and paucity of tissue-specific gene expression on the *Drosophila* X chromosome. *BMC Biol*. 2011;9:29. <https://doi.org/10.1186/1741-7007-9-29> PMID: 21542906
63. Meisel RP, Malone JH, Clark AG. Disentangling the relationship between sex-biased gene expression and X-linkage. *Genome Res*. 2012;22(7):1255–65. <https://doi.org/10.1101/gr.132100.111> PMID: 22499666
64. Bachtrog D. Y-chromosome evolution: emerging insights into processes of Y-chromosome degeneration. *Nat Rev Genet*. 2013;14(2):113–24. <https://doi.org/10.1038/nrg3366> PMID: 23329112
65. Turner JMA. Meiotic Silencing in Mammals. *Annu Rev Genet*. 2015;49:395–412. <https://doi.org/10.1146/annurev-genet-112414-055145> PMID: 26631513
66. Viera A, Parra MT, Arévalo S, García de la Vega C, Santos JL, Page J. X Chromosome Inactivation during Grasshopper Spermatogenesis. *Genes (Basel)*. 2021;12(12):1844. <https://doi.org/10.3390/genes12121844> PMID: 34946793

67. Schoenmakers S, Wassenaar E, Hoogerbrugge JW, Laven JSE, Grootegoed JA, Baarends WM. Female meiotic sex chromosome inactivation in chicken. *PLoS Genet.* 2009;5(5):e1000466. <https://doi.org/10.1371/journal.pgen.1000466> PMID: [19461881](https://pubmed.ncbi.nlm.nih.gov/19461881/)
68. Mahadevaraju S, Fear JM, Akeju M, Galletta BJ, Pinheiro MMLS, Avelino CC, et al. Dynamic sex chromosome expression in *Drosophila* male germ cells. *Nat Commun.* 2021;12(1):892. <https://doi.org/10.1038/s41467-021-20897-y> PMID: [33563972](https://pubmed.ncbi.nlm.nih.gov/33563972/)
69. Witt E, Shao Z, Hu C, Krause HM, Zhao L. Single-cell RNA-sequencing reveals pre-meiotic X-chromosome dosage compensation in *Drosophila* testis. *PLoS Genet.* 2021;17(8):e1009728. <https://doi.org/10.1371/journal.pgen.1009728> PMID: [34403408](https://pubmed.ncbi.nlm.nih.gov/34403408/)
70. Raz AA, Vida GS, Stern SR, Mahadevaraju S, Fingerhut JM, Viveiros JM, et al. Emergent dynamics of adult stem cell lineages from single nucleus and single cell RNA-Seq of *Drosophila* testes. *Elife.* 2023;12:e82201. <https://doi.org/10.7554/eLife.82201> PMID: [36795469](https://pubmed.ncbi.nlm.nih.gov/36795469/)
71. Anderson J, Henikoff S, Ahmad K. Chromosome-specific maturation of the epigenome in the *Drosophila* male germline. *eLife Sciences Publications, Ltd.* 2023.
72. McKee BD, Handel MA. Sex chromosomes, recombination, and chromatin conformation. *Chromosoma.* 1993;102(2):71–80. <https://doi.org/10.1007/BF00356023> PMID: [8432196](https://pubmed.ncbi.nlm.nih.gov/8432196/)
73. McKee BD, Habera L, Vrana JA. Evidence that intergenic spacer repeats of *Drosophila melanogaster* rRNA genes function as X-Y pairing sites in male meiosis, and a general model for achiasmatic pairing. *Genetics.* 1992;132(2):529–44. <https://doi.org/10.1093/genetics/132.2.529> PMID: [1330825](https://pubmed.ncbi.nlm.nih.gov/1330825/)
74. Kelly WG, Schaner CE, Dernburg AF, Lee M-H, Kim SK, Villeneuve AM, et al. X-chromosome silencing in the germline of *C. elegans*. *Development.* 2002;129(2):479–92. <https://doi.org/10.1242/dev.129.2.479> PMID: [11807039](https://pubmed.ncbi.nlm.nih.gov/11807039/)
75. Deng X, Hiatt JB, Nguyen DK, Ercan S, Sturgill D, Hillier LW, et al. Evidence for compensatory upregulation of expressed X-linked genes in mammals, *Caenorhabditis elegans* and *Drosophila melanogaster*. *Nat Genet.* 2011;43(12):1179–85. <https://doi.org/10.1038/ng.948> PMID: [22019781](https://pubmed.ncbi.nlm.nih.gov/22019781/)